Pergamon

J. Mech. Phys. Solids, Vol. 45, No. 9, pp. 1473–1493, 1997
© 1997 Elsevier Science Ltd
Printed in Great Britain. All rights reserved
0022-5096/97 $17.00+0.00

PII: S0022-5096(97)00013-6

A FINITE ELEMENT ANALYSIS OF THE MOTION AND EVOLUTION OF VOIDS DUE TO STRAIN AND ELECTROMIGRATION INDUCED SURFACE DIFFUSION

L. XIA†, A. F. BOWER‡, Z. SUO§ AND C. F. SHIH†

† Division of Engineering, Brown University, Providence, RI 02912, U.S.A. § Mechanical and Environmental Engineering Department, Materials Department, University of California, Santa Barbara, CA 93106, U.S.A.

(*Received* 19 *August* 1996; *in revised form* 18 *February* 1997)

ABSTRACT

Microelectronic circuits often fail because cracks and voids cause open circuits in their interconnects. Many of the mechanisms of failure are believed to be associated with diffusion of material along the surfaces, interfaces or grain boundaries in the line; material may also flow through the lattice of the crystal. The diffusion is driven by variations in elastic strain energy and stress in the solid, and by the flow of electric current. To predict the conditions necessary for failure to occur in an interconnect, one must account for the influence of both deformation and electric current flow through the interior of the solid, and also for the effects of mass flow. To this end, we describe a two dimensional finite element method for computing the motion and evolution of voids by surface diffusion in an elastic, electrically conducting solid. Various case studies are presented to demonstrate the accuracy and capabilities of the method, including the evolution of a void towards a circular shape due to diffusion driven by surface energy, the migration and evolution of a void in a conducting strip due to electromigration induced surface diffusion, and the evolution of a void in an elastic solid due to strain energy driven surface diffusion. © 1997 Elsevier Science Ltd.

Keywords: A. diffusion, surface, A. electromigration, B. elastic material, C. finite elements.

1. INTRODUCTION

Microelectronic circuits contain thin lines of aluminium alloy, which make electrical contact between neighboring devices on the chip. A typical interconnect line has a rectangular cross-section, with dimensions of the order 2×0.5 μm, as shown in Fig. 1. It would be desirable to reduce these dimensions still further, but efforts to do so have been impeded by frequent mechanical failure in the lines. Interconnects almost always contain defects such as voids and cracks, and if a defect is large enough to sever the line, it causes an open circuit. This form of failure has become significantly more common as the dimensions of interconnect lines have been reduced, so there is great interest in identifying the mechanisms responsible for nucleating and propagating voids in interconnects, and in finding ways to reduce the likelihood of failure.

The material in an interconnect line is subjected to mechanical stress, which provides

‡ To whom correspondence should be addressed.

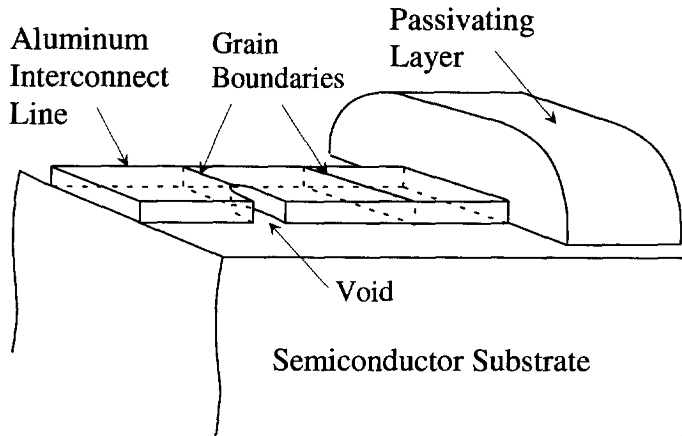

Fig. 1. Features of a typical interconnect line.

one driving force for void nucleation and growth. Interconnects are usually deposited on a semiconductor substrate, and covered with a thick layer of oxide. This passivating layer is deposited at high temperature (400°C is typical), and the device operates at a lower temperature (100°C). Since the thermal expansion coefficient of aluminium is of the order $20 \times 10^{-6}\ \mathrm{K}^{-1}$, while that of the surrounding material is $5 \times 10^{-6}\ \mathrm{K}^{-1}$, large tensile stresses are induced in the line by the manufacturing process. One may estimate the magnitude of the stresses by assuming that the solid remains elastic: this suggests that the vertical stress $\sigma_z \sim 200$ MPa; the lateral stress $\sigma_x \sim 800$ MPa, and the longitudinal stress $\sigma_y \sim 900$ MPa (Korhonen *et al.*, 1991a). These stresses are sufficient to induce plastic deformation in the line, and indirect experimental evidence suggests that voids are nucleated when the solid is cooled to room temperature after passivation (Korhonen *et al.*, 1991b). The most common nucleation site appears to be where grain boundaries intersect the edge of the line, but voids are also observed away from the line edges, and near the center of the grains. Because of the constraining effect of the semiconductor substrate and the overlying oxide layer, the voids are initially small compared to the width of the line. However, they continue to grow, migrate and change their shape during service. Diffusion plays a central role in this process: voids may change their shape due to surface diffusion, while material may be removed from a void by grain boundary and lattice diffusion.

During service, a dense electric current flows through interconnect lines. Current densities of 10^5 A cm^{-2} are typical; accelerated tests are often performed at current densities up to 10^7 A cm^{-2}. The current flow has a number of consequences. It heats the line, which increases the rate of diffusion and may also affect the thermal stress distribution. The current also causes material to diffuse along the line, due to a phenomenon known as electromigration. In aluminium, material diffuses in a direction opposite to the electric current, at a rate approximately proportional to the current density. The rate of material flow is not uniform along the length of the line, due to irregularities in the microstructure or geometry of the line, and due to temperature gradients. Material therefore tends to accumulate in some sections of the

line, and is removed from others. This induces severe stresses in both the interconnect and the surrounding material, which may cause the material surrounding the line to crack and also increase the rate of stress induced void growth in the line. Voids may grow as a direct result of electromigration, since the electric current may cause material to diffuse away from the voids along grain boundaries. Electromigration can also cause voids to translate along an interconnect line, by relocating material from one side of the cavities to the other (Ho, 1970). In-situ TEM and SEM observations show that voids travel large distances along the line, and constantly change their shape as they do so (Marieb *et al.*, 1994; Riege *et al.*, 1995). Small voids travel more quickly than large ones, and void coalescence has been observed as one mechanism leading to open circuits. A void can also sever a line by changing its shape. Most voids in interconnects are well rounded, and an interconnect can contain a large number of such voids without serious consequences. However, a few voids resemble narrow cracks, oriented perpendicular to the line, and are often found to cause open circuits. The origin of these crack like voids is not fully understood, but it has been suggested that high stresses and high electric fields can cause a rounded void to collapse into a crack, by a process involving surface diffusion (Arzt *et al.*, 1994; Yang *et al.*, 1994).

There is hope that interconnect failures may be avoided by designing the microstructure and geometry of the line appropriately. For example, it has been shown that lines with a "bamboo" grain structure, with grain boundaries oriented perpendicular to the line direction as shown in Fig. 1, are resistant to failure. Some success has also been reported using single-crystal lines (Hasunuma *et al.*, 1995). Computational techniques such as the finite element method offer an inexpensive and versatile way to design against failure, and conventional finite element methods have been used successfully to analyze stress and damage in interconnect lines. However, there are several phenomena which play an important role in interconnect failures, that are not considered in standard techniques for structural failure analysis. The effects of stress and electromigration induced diffusion are particularly difficult to model.

Some progress has been made in developing finite element methods to solve problems involving coupled diffusion and deformation. Needleman and Rice (1980) derived a variational principle governing grain boundary diffusion and plastic flow in a rigid-power law creeping solid, which they used as the basis for a finite element analysis of grain boundary cavitation. Their approach has since been extended and applied to a range of problems involving grain boundary diffusion by Cocks and co-workers (Cocks, 1989; Cocks and Searle, 1991; Pan and Cocks, 1995; Cocks and Gill, 1996); the method has also been used to investigate void growth by grain boundary diffusion in interconnect lines (Bower and Freund, 1993). Recently, Bower and Freund (1995) developed a numerical scheme specifically intended to model electromigration in deformable solids. They used the finite element method to solve the coupled equation governing diffusion, deformation and electric current flow through the solid. The analysis accounted for the effects of both grain boundary and surface diffusion, as well as elastic or creep deformation within the interconnect. The model was able to predict many of the features that have been observed in interconnects, including void migration, changes in void shape and electromigration induced stress and plastic deformation.

In this paper, we have extended the finite element method described in Bower and

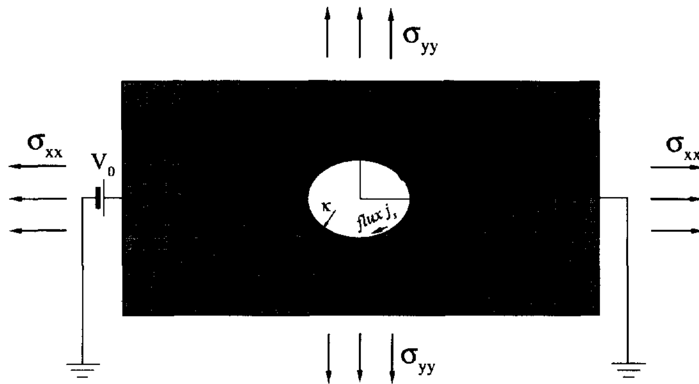

Fig. 2. A void in an electrically conducting, elastic solid.

Freund (1995) so as to solve the problems involving pure surface diffusion in electrically conducting, linear elastic solids. In particular, we have developed a new approach to integrating the surface diffusion equations; we have implemented an improved mesh adaption strategy; and we have included the influence of elastic strain energy in driving surface diffusion. We will demonstrate that the method is effective and accurate by applying it to a range of case studies. Furthermore, it is straightforward to extend the method to situations involving inelastic deformation, and to account for additional phenomena such as heat generation and flow in the solid.

The problem to be solved is illustrated in Fig. 2. We idealize the interconnect line as a linear elastic solid, which conducts electric current according to Ohm's law. The solid is loaded mechanically by subjecting its boundary to a prescribed distribution of traction or displacement, while an electric field is induced in the line by prescribing either the voltage or the electric current density on its boundaries. We assume that the line deforms in a state of plane strain, and that the displacements are infinitesimal; similarly, we assume that the electric field in the line has no component normal to the plane of the figure. The line may contain one or more voids, whose initial shape is assumed to be known.

The electric field in the line, together with the elastic strain energy, give rise to an externally induced driving force for diffusion in the solid. Diffusion is also driven by the surface or bulk free energy of the material. Atoms tend to diffuse from regions of high chemical potential to those of low chemical potential, and so cause a change in shape of the stress free reference configuration of the solid. In practice, matter may diffuse through the crystal lattice, along surfaces and through grain boundaries. However, the rate of diffusion is generally much greater along surfaces and grain boundaries than through the lattice, so we have chosen to neglect bulk difficulties in our analysis. For simplicity, we have also assumed that the line contains no grain boundaries: diffusion is therefore confined to the surface of the void.

Surface diffusion may cause voids in the line to change their shape. In the absence of external mechanical or electrical loading, the void will approach the shape that minimizes the total surface free energy. We have assumed that the surface energy of the solid is isotropic, in which case the energy minimizing shape is a cylinder. When

the solid is loaded, the electric field and elastic strain energy also drive diffusion on the void surface, and may cause the void to drift through the solid and to change its shape.

We will describe a finite element procedure which can be used to compute the resulting behavior of the void. The convergence and accuracy of the method will be illustrated by comparing its predictions to exact solutions. We will then present several case studies to illustrate the effects of stress and electromigration induced surface diffusion on voids in interconnect lines.

Our objective in this paper is to describe methods that may be used to model some of the failure mechanisms in interconnect lines, rather than to conduct an exhaustive study of the failure mechanisms themselves. Many of our assumptions are unrealistic: for example, we have neglected the influence of inelastic deformation, have ignored the effects of grain boundaries and have assumed plane deformation. These issues are promising areas for future research.

2. GOVERNING EQUATIONS

We begin by outlining the assumptions that we have made in our analysis. Consider the idealized interconnect line shown in Fig. 2. Our objective is to compute the stress and deformation induced in the solid by the mechanical loads; to find the distribution of electric field and current in the line, and to deduce the resulting change in shape of the void.

The void changes its shape because atoms diffuse over its surface. In addition, the deformation induced by mechanical loading will cause a displacement of material points on the void surface. In this work we have assumed that the solid is elastic so that the displacements due to mechanical loading are small. Therefore, changes in shape caused by deformation do not influence diffusion on the void surface.

In the absence of electrical current, surface diffusion is driven by a variation in chemical potential, which causes atoms to migrate from regions of high chemical potential to those of low chemical potential. There are two contributions to the chemical potential of an atom on a free surface. The first is associated with the free energy of the surface, while the second is due to the elastic strain energy stored in the volume of material associated with an atom. Thus

$$\mu = \mu_0 + \Omega(\phi - \gamma_s \kappa), \tag{2.1}$$

where μ_0 is the chemical potential of the bulk; Ω is the atomic volume, $\phi = \frac{1}{2}\sigma_{ij}\varepsilon_{ij}$ is the elastic strain energy density, γ_s is the surface energy and κ is the curvature of the surface. The sign convention for κ is such that a concave surface (such as a void surface) has positive curvature; a convex surface (a hillock, for example) has negative curvature. We assume that the rate of mass transport is proportional to the gradient in potential. If an electric current flows down the line, it gives rise to an additional driving force for diffusion: the mass flow rate due to electromigration is taken to be proportional to the component of electric field tangent to the surface. Thus, the total flux on a void surface may be expressed as

$$j_s = -\mathscr{D}_s\left(\frac{\partial \mu}{\partial s} - |e|Z^*\frac{\partial V}{\partial s}\right), \tag{2.2}$$

where s denotes the arc length measured from some convenient point on the void surface; j_s is the volume of material which crosses a line of unit length perpendicular to the (x, y) plane per unit time; $\partial\mu/\partial s$ denotes the gradient in chemical potential along the void surface; V is the electrical potential, $-\partial V/\partial s$ is the electric field tangent to the surface; e is the charge of an electron; Z^* is the "effective valence" of an atom (a phenomenological constant which is positive for aluminium); and $\mathscr{D}_s$ is a temperature dependent constant, related to the coefficient of surface diffusion by

$$\mathscr{D}_s = \frac{D_s\delta_s}{kT}e^{-Q_s/kT}. \tag{2.3}$$

In (2.3), $D_s \exp(-Q_s/kT)$ is the surface diffusion coefficient and δ_s is the thickness of the diffusion layer. Q_s is the activation energy for surface diffusion, T is the temperature and k is the Boltzmann constant.

The rate at which material is deposited or removed from an element is related to the divergence of the surface flux by mass conservation. Thus, the normal velocity of the surface of the void in the reference configuration is

$$v_n = -\frac{\partial j_s}{\partial s}. \tag{2.4}$$

Combining (2.2) and (2.4) shows that

$$j_s = -\mathscr{D}_s\left(\Omega\frac{\partial \phi}{\partial s} - \gamma_s\Omega\frac{\partial \kappa}{\partial s} - |e|Z^*\frac{\partial V}{\partial s}\right), \tag{2.5}$$

$$v_n = \mathscr{D}_s\left(\Omega\frac{\partial^2 \phi}{\partial s^2} - \gamma_s\Omega\frac{\partial^2 \kappa}{\partial s^2} - |e|Z^*\frac{\partial^2 V}{\partial s^2}\right). \tag{2.6}$$

To compute the flux on the void surface and the resulting motion of its boundary, one must determine the distribution of strain energy and electric field in the solid. The deformation induced by the mechanical loading may be described by the displacement field $u_i(x_j)$ of material points from the stress free configuration of the solid. Then, the deformation may be characterized by the infinitesimal strain

$$\varepsilon_{ij} = \tfrac{1}{2}(u_{i,j} + u_{j,i}), \tag{2.7}$$

where the comma denotes partial differentiation with respect to a spatial coordinate, in the usual manner. We have assumed that the interconnect is an isotropic, linear elastic solid, so the stress field is related to the strains by

$$\sigma_{ij} = \frac{E}{1+\nu}\left(\varepsilon_{ij} + \frac{\nu}{1-2\nu}\varepsilon_{kk}\delta_{ij}\right),$$

where E and ν denote Young's modulus and Poisson's ratio, respectively. The stress field in the solid must be in mechanical equilibrium, which requires

$$\sigma_{ij,j} = 0. \tag{2.8}$$

We assume that the solid deforms in a state of plane strain, with displacement components u_1 and u_2 independent of x_3, and $u_3(x_1, x_2) = 0$. The displacements are prescribed over parts of the boundary $\partial_1\mathscr{R}$, while the tractions $t_i = \sigma_{ij}n_j$ are prescribed over the remainder of the boundary $\partial_2\mathscr{R}$. The surface of the void is free from tractions. These conditions are sufficient to determine the displacement, strain and stress fields in the solid. Subsequently, the distribution of elastic strain energy $\phi = \frac{1}{2}\sigma_{ij}\varepsilon_{ij}$ may be deduced.

One must also determine the electric field in the solid. Suppose that $V(x_i)$ denotes the electrical potential at a point (x_1, x_2, x_3); let ρ be the electrical resistivity of the material, and denote the components of current density in the line by $J_i(x_k)$. Ohm's law and charge conservation require that

$$\rho J_i = -V_{,i} \quad J_{i,i} = 0. \tag{2.9}$$

We assume that the current flows only in the (x_1, x_2) plane, which requires $V_{,3} = 0$. The distribution of voltage is prescribed over the ends of the line, while the normal component of current density $J_i n_i$ is assumed to vanish on the remainder of the boundary. In particular, $J_i n_i = 0$ on the void surface.

3. NUMERICAL PROCEDURE

We have used a finite element procedure to solve the equations outlined in the preceding section. It is convenient to perform the calculation in three separate steps. Consider the interconnect sketched in Fig. 2. Suppose that the shape of the stress free reference configuration for the solid at time t is known: our objective is to calculate the deformation and diffusion in the solid that occur during a subsequent infinitesimal time interval Δt. The first step is to calculate the distribution of voltage $V(x_i)$ in the solid at time t. Secondly, we compute the change in displacement field u_i and stress field σ_{ij} as a result of mechanical loading and diffusion in the solid. To do so, we solve the equations of mechanical equilibrium and the diffusion equations, using the configuration at time t as a reference. Finally, we update the shape of the voids, which change their shape as a result of diffusion.

We have used a standard procedure to calculate the distribution of voltage. Equation (2.9) is written in its weak form

$$\int_{\mathscr{R}} \frac{1}{\rho} V_{,i}\delta V_{,i}\,\mathrm{d}A + \int_{\partial\mathscr{R}} J_i n_i \delta V\,\mathrm{d}s = 0, \tag{3.1}$$

where $\mathscr{R}$ denotes the two dimensional region occupied by the solid, $\partial\mathscr{R}$ denotes its boundary and δV is an admissible variation in voltage, which satisfies $\delta V = 0$ on regions of the boundary where voltage is prescribed. Equation (3.1) must hold for all such δV. It is straightforward to solve this equation using a standard finite element method. We have found it convenient to approximate the distribution of voltage using six noded (quadratic) triangular elements, since the mesh may then be generated automatically, using an advancing front algorithm (Peraire *et al.*, 1987).

The equations of mechanical equilibrium may also be solved using the standard finite element method. In the usual way, we calculate the displacement field u_i and stress field σ_{ij} that satisfy

$$\int_{\mathscr{R}} \sigma_{ij}\delta u_{i,j}\, \mathrm{d}A = \int_{\partial\mathscr{R}} t_i \delta u_i\, \mathrm{d}s \tag{3.2}$$

for all variations in displacement δu_i satisfying $\delta u_i = 0$ on $\partial_1\mathscr{R}$. It is convenient to interpolate both V and u_i with the same finite element mesh, so (3.2) is also reduced to a discrete form using quadratic triangular finite elements.

Finally, we solve the surface diffusion equation to deduce the change in shape of the void during the time interval Δt. We have devised two finite element based procedures to do this. In the first method, we write a weak form of (2.6) directly,

$$\int_{\Gamma} v_{\mathrm{n}} \delta v_{\mathrm{n}}\, \mathrm{d}s = \int_{\Gamma} \mathscr{D}_{\mathrm{s}}(\Omega\phi - \gamma_{\mathrm{s}}\Omega\kappa - |e|Z^* V)\frac{\partial^2 \delta v_{\mathrm{n}}}{\partial s^2}\, \mathrm{d}s, \tag{3.3}$$

and solve for the surface velocity which satisfies (3.3) for all admissible variations δv_n. Our second approach uses a mixed formulation: instead of computing v_{n} directly, we calculate the flux j_{s} by enforcing (2.5) in its weak form

$$\int_{\Gamma} j_{\mathrm{s}} \delta j_{\mathrm{s}}\, \mathrm{d}s = \int_{\Gamma} \mathscr{D}_{\mathrm{s}}(\Omega\phi - \gamma_{\mathrm{s}}\Omega\kappa - |e|Z^* V)\frac{\partial \delta j_{\mathrm{s}}}{\partial s}\, \mathrm{d}s, \tag{3.4}$$

which must hold for all admissible variations in flux δj_{s}. The surface velocity v_{n} is then determined from (2.4). This formulation has the advantage that mass conservation is enforced over the entire surface of the void, whereas the expression given in (3.3) guarantees only that the total mass of the solid is conserved. This improvement is obtained at the cost of having to interpolate j_{s} with continuously differentiable shape functions.

To compute the change in shape of the void, one must integrate either (3.3) or (3.4) with respect to time. The equations are stiff, owing to the term involving the curvature of the void surface. We have integrated them using a semi-implicit Euler scheme. Let $\Delta h(s)$ denote the normal displacement of the void surface in the reference configuration during the time interval Δt. In a forward-Euler time integration scheme, one would set $\Delta h = \Delta t v_n(t)$, where the normal velocity of the void surface is obtained by solving (3.3) or (3.4) at time t. We have found that this algorithm is stable only if the time step Δt is prohibitively small. Much larger time steps may be taken if we use a first-order predictor for the curvature of the void. Let κ_0 denote the curvature of the surface at time t. Then, the curvature at time $t+\Delta t$ may be estimated as

$$\kappa(t+\Delta t) = \kappa_0 + \frac{\partial^2 \Delta h}{\partial s^2} + \kappa_0^2 \Delta h + \mathscr{O}(\Delta h^2). \tag{3.5}$$

To compute v_n or j_s from (3.3) or (3.4), we approximate the curvature using

$$\kappa = (1-\alpha)\kappa_0 + \alpha\kappa(t+\Delta t), \tag{3.6}$$

where $0 \leqslant \alpha \leqslant 1$ is an adjustable parameter controlling the integration scheme, and

$\kappa(t+\Delta t)$ is estimated using (3.5). Setting $\alpha = 0$ reduces the integration formula to the standard explicit forward-Euler scheme, while $\alpha = 1$ represents the first iteration in a fully implicit integration scheme. As usual, the integration scheme is most stable with $\alpha = 1$, while $\alpha \approx 0.5$ appears to give the best accuracy. In most of the simulations to be presented here, we have set $\alpha = 1$.

Finally, substituting (3.5) and (3.6) into (3.3) or (3.4) shows that the change in shape of the void may be computed either by solving

$$\int_\Gamma \Delta h \delta v_n + \alpha \Delta t \mathscr{D}_s \gamma_s \Omega \left(\frac{\partial^2 \Delta h}{\partial s^2} + \kappa_0^2 \Delta h \right) \frac{\partial^2 \delta v_n}{\partial s^2} \mathrm{d}s = \int_\Gamma \Delta t \mathscr{D}_s (\Omega \phi - \gamma_s \Omega \kappa_0 - |e| Z^* V) \frac{\partial^2 \delta v_n}{\partial s^2} \mathrm{d}s \quad (3.7)$$

for Δh directly, or else by finding the flux j_s which satisfies

$$\int_\Gamma j_s \delta j_s - \alpha \Delta t \mathscr{D}_s \gamma_s \Omega \left(\frac{\partial^3 j_s}{\partial s^3} + \kappa_0^2 \frac{\partial j_s}{\partial s} \right) \frac{\partial \delta j_s}{\partial s} \mathrm{d}s = \int_\Gamma \mathscr{D}_s (\Omega \phi - \gamma_s \Omega \kappa_0 - |e| Z^* V) \frac{\partial \delta j_s}{\partial s} \mathrm{d}s, \quad (3.8)$$

and then computing the normal displacement from $\Delta h = -\Delta t \partial j_s / \partial^s$.

We have used these results to develop a finite element method for computing the shape of a void in an interconnect. At time $t = 0$, the initial shape of the void is specified by a set of "control points" on its perimeter; other boundaries of the solid are described in the same way. The geometry of the solid is then interpolated between these points, using cubic parametric splines. The analysis begins by generating a mesh of six noded, triangular elements to fill the region occupied by the solid. We have found the advancing front algorithm described by Peraire *et al.* (1987) to be particularly effective for this purpose. In this approach, each boundary is first subdivided into a set of faces, which connect a set of boundary nodes. This set of faces is termed the initial "front". Triangular elements are then created, starting from the smallest face on the front. This face is taken as the base of the new element, and the triangle is formed either by identifying a suitable node on the front which should form its vertex, or by generating a new node. If a new node is introduced, its position is chosen so as to generate an element with a specified height. Once the triangle has been generated, the front is updated: segments on the existing front which coincide with one of the sides of the new triangle are removed, while new sides of the triangle are added to the front. This procedure is repeated until there are no faces left on the front. The quality of the final mesh is improved by shifting the position of each node in the mesh slightly, using Laplacian smoothing (Cavendish, 1974). Finally, mid-side nodes are added to each triangle to form six noded quadratic elements. We have used the data structures and operations suggested by Lohner (1988) to ensure an efficient implementation of the algorithm.

The advancing front algorithm allows one to generate a mesh with a variable element size. In most of the computations described here, we have used a particularly simple approach to control the mesh density. The size of the faces which form the initial front on the void surface are controlled by the local value of the strain energy

density on the surface (a uniform mesh is sufficient for many simulations). When elements are generated along the front, the height of each triangle is taken to be somewhat greater than its base. This procedure generates a fine mesh around the void, and a coarse mesh away from it.

Once a mesh has been generated, the standard finite element method is then used to compute values of voltage and displacement at each node on this mesh; nodal values of strain energy density are also determined, either by extrapolating the values from the integration points of each element, or using a variational recovery procedure (Oden and Reddy, 1973; Hinton and Campbell, 1974).

Next, we calculate the change in shape of the void surface during a time interval Δt, by solving (3.7) or (3.8) using a finite element procedure. The corner nodes and element faces on the surface of the void are taken to comprise a one dimensional finite element mesh for interpolating field variables in (3.7) or (3.8). The initial curvature κ_0 is determined at each node by fitting a parametric cubic spline through the nodes on the boundary. The voltage and strain energy densities are transferred from the mesh in the interior of the solid. To solve (3.7), we approximate Δh and δv_n within each element by interpolating between values at the nodes. Note that for the finite element procedure to converge, one must chose interpolation functions such that both Δh and $\partial(\Delta h)/\partial s$ are continuous across neighboring elements; δv_n must be interpolated in the same way. We therefore approximate $\Delta h(s)$ using a piecewise cubic Hermitian interpolation between the values of Δh and its derivative $\partial(\Delta h)/\partial s$ at each node, and use a similar procedure for δv_n. The values of κ_0, ϕ and V within each element are determined using a piecewise linear interpolation between their nodal values. Equation (3.7) is then reduced to a system of linear equations which may be solved for the nodal values of Δh and $\partial(\Delta h)/\partial s$.

Equation (3.8) may be solved for j_s using a similar approach. In this case, the flux j_s must be interpolated so that j_s and both its first and second derivatives are continuous across neighboring elements. We therefore approximate j_s using a piecewise quintic Hermitian interpolation between nodal values of j_s and $\partial j_s/\partial s$. The shape functions are recorded in the Appendix for convenience. The curvature, voltage and strain energy density are approximated using a piecewise linear interpolation between the nodes, as before. This reduces equation (3.8) to a system of linear equations which may be solved for the nodal values of j_s and $\partial j_s/\partial s$. Finally, we compute the change in position of each node on the void surface from the nodal values of $\partial j_s/\partial s$, using $\Delta h = -\Delta t \partial j_s/\partial s$.

The results are used to update the coordinates of nodes on the surface of the void. The nodes on each boundary of the solid are then taken as new control points, which specify the geometry of the solid at time Δt. A new finite element mesh may then be generated in the interior of the solid, and the procedure is repeated to compute the progressive change in shape of the void.

The time step Δt must be chosen with care: our algorithm for integrating the surface diffusion equations with respect to time is conditionally stable. The stability of the algorithm is greatly improved if the numerical parameter $\alpha = 1$; nevertheless, instabilities may still occur if Δt is too large. The difficulty is caused by the terms involving curvature in (3.7) and (3.8): small changes in the positions of the points on the void surface can lead to large changes in curvature, so small time steps must be taken to

compute the rate of change of curvature accurately. The electric and elastic fields in the solid change more slowly as the surface of the void evolves. Consequently, subcycling may be used to speed up the numerical procedure. The electric and elastic fields in the solid are computed once; then, the surface diffusion equation is solved several times with a small time step. The curvature of the void surface κ_0 is updated each time the equation is solved, but the values of voltage or elastic strain energy are updated less frequently. We have found that using between 10 and 100 subcycles between each computation of the elastic or electric fields gives good results.

4. RESULTS AND DISCUSSION

We describe several case studies to demonstrate the accuracy of our numerical procedure and to illustrate its capabilities.

4.1. *Diffusion under surface tension alone*

For the first example, consider a solid which contains an initially elliptical void, and assume that the solid is free of stress and electric current. In this case, surface diffusion is driven only by the surface free energy of the solid, and the void changes its shape so as to reduce its surface area. This behavior is illustrated in Fig. 3: the initial void has semiaxes with $b/a = 0.1$, and the profile of the void is shown at equally spaced time intervals $\Delta t\mathscr{D}_s\Omega\gamma_s/a^4 = 0.0004$, where $\Delta t\mathscr{D}_s\Omega\gamma_s/a^4$ is a dimensionless measure of time. As expected, the stable profile of the void is a circle. An exact solution to this problem is not available, but we may use the initial velocity of the surface of the void as a check on the accuracy of our numerical method. For an ellipse with a profile given by

$$x = a\cos\theta \quad y = b\sin\theta \tag{4.1}$$

the curvature is

$$\kappa_0 = \frac{ab}{(a^2\sin^2\theta + b^2\cos^2\theta)^{3/2}}, \tag{4.2}$$

so that the normal velocity of the surface of the ellipse follows as

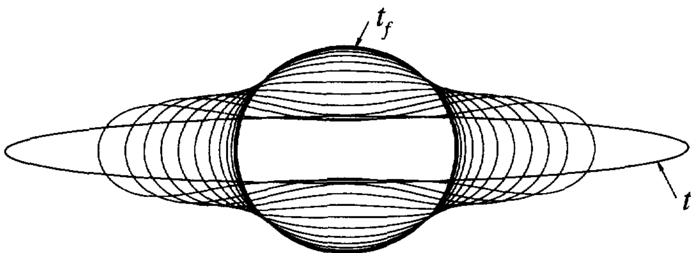

Fig. 3. A cavity with an initially elliptical profile, evolving due to diffusion driven by surface energy. The ellipse has semiaxes $a/b = 0.1$, and profiles are shown at equally spaced intervals $\Delta t\mathscr{D}_s\Omega\gamma_s/a^4 = 0.0004$.

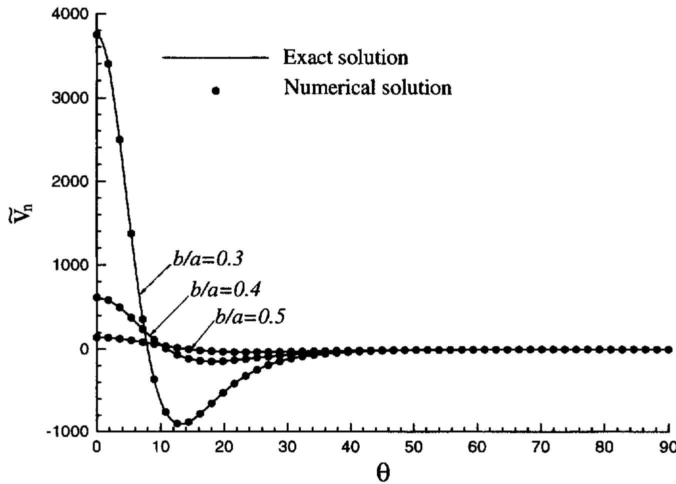

Fig. 4. The initial velocity of the surface of an elliptical void which evolves due to diffusion driven by surface energy. The velocity is expressed in dimensionless form as $\tilde{v}_n = v_n a^3/\mathscr{D}_s\Omega\gamma_s$.

$$v_n = 3\mathscr{D}_s\Omega\gamma_s(b^2-a^2)ab\frac{[a^2\sin^2\theta(1+4\cos^2\theta)-b^2\cos^2\theta(1+4\sin^2\theta)]}{(a^2\sin^2\theta+b^2\cos^2\theta)^{9/2}}. \tag{4.3}$$

Figure 4 shows the exact value of the dimensionless velocity $\tilde{v}_n = v_n a^3/\Omega\mathscr{D}_s\gamma_s$ for ellipses with initial semiaxes in the ratio $b/a = 0.3$, 0.4 and 0.5. The result obtained using the finite element interpolation of (3.8) is shown as a set of symbols for comparison. We have not shown results obtained using (3.7), since they are virtually indistinguishable from the results obtained by interpolating fluxes, (3.8).

The elliptical cavity provides a convenient solution to check the convergence of the finite element solution to the surface diffusion equations. Define a measure of error

$$\mathscr{E} = \left\{\frac{1}{L}\int_0^L (v_n^{\text{exact}} - v_n^{\text{numerical}})^2/[v_n^{\max}]^2\,ds\right\}^{1/2}, \tag{4.4}$$

where L denotes the circumference of the ellipse; v_n^{exact} is computed from (4.3); $v_n^{\max}$ is the maximum value of v_n^{exact}; and the numerical solution is obtained using the finite element interpolation of (3.7) or (3.8). Figure 5 shows the variation of $\mathscr{E}$ with the number of (uniformly spaced) elements used in the finite element interpolation, for solutions based on both (3.7) and (3.8). The result shows that both methods tend to converge at a similar rate, but for a given number of elements, the solution obtained by interpolating flux j_s and its derivative (3.8) appears to be somewhat more accurate than that based on (3.7). We therefore used this approach to obtain the remaining results in this paper. For very large numbers of elements ($N > 1000$), the rate of convergence of the solution obtained using (3.8) decreases; for $N > 10{,}000$ we have observed a similar reduction in the rate of convergence of the method based on (3.7). We believe that this is a consequence of rounding errors.

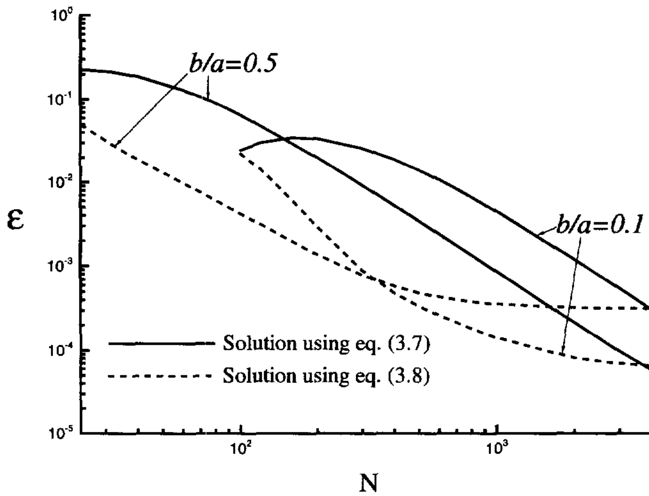

Fig. 5. Illustrating the convergence of the finite element solution to the surface diffusion equations. The measure of error is defined in (4.4).

4.2. *Electromigration driven voids*

For our second test, we investigate the behavior of a void in an electrically conducting strip (Fig. 6). The strip has length L and height H; at time $t = 0$, a cavity with radius a lies on the symmetry axis of the strip. An electric current is induced in the solid by prescribing the voltage on both its ends: $V = V_0$ on $x = 0$, and $V = 0$ on $x = L$. The solid is free of mechanical stress. The current flow causes material to diffuse from one side of the cavity to the other, so the void appears to migrate through the strip. If the radius of the void is small compared to the dimensions of the strip, then the cavity remains circular, and its speed may be calculated exactly (Ho, 1970):

$$V_{\text{cavity}} = 2\frac{\mathscr{D}_s|e|Z^*E^\infty}{a}, \tag{4.5}$$

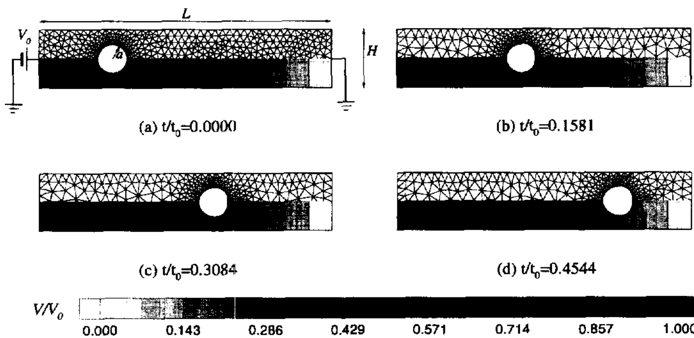

Fig. 6. Stable migration of a void in a stress free, electrically conducting strip. Results are shown for $\chi = 10$ [equation (4.6)]; $a/H = 0.25$; $L/H = 5$. The characteristic time $t_0 = a^4/\mathscr{D}_s\Omega\gamma_s$; the contours show voltage.

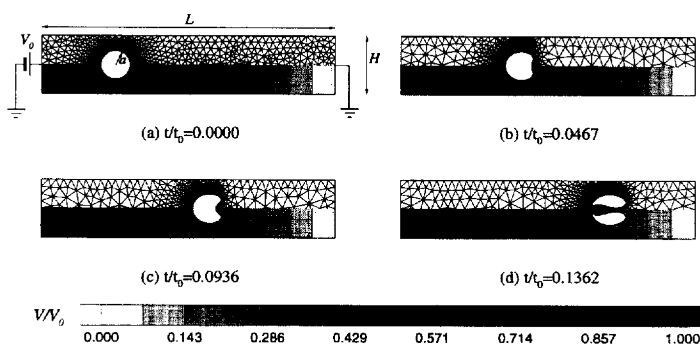

Fig. 7. A void in a stress free, electrically conducting strip, as it collapses into slits. Results are shown for $\chi = 30$ [equation (4.6)]; $a/H = 0.25$; $L/H = 5$. The characteristic time is $t_0 = a^4/\mathscr{D}_s\Omega\gamma_s$; the contours show voltage.

where $E^\infty = V_0/L$ is the electric field remote from the void. For large values of H/a and L/a, our numerical solution is within 1% of the exact solution.

The void remains circular, as long as it is small compared to the width of the line. If the diameter of the void is comparable to the line width, the void tends to adopt a spade shape, as shown in Fig. 6. The void shape is then governed by two dimensionless parameters: the ratio of void size to line width a/H and a parameter χ which specifies the ratio of the electromigration driving force to the driving force associated with surface energy (Wang *et al.*, 1996),

$$\chi = V_0|e|Z^*a^2/\Omega\gamma_s L. \tag{4.6}$$

For low values of χ, the driving force associated with surface energy dominates over the electromigration force, so the void tends to remain circular. For high values, the electromigration driving force causes a significant change in shape.

If the parameter χ exceeds a critical value, one finds that an initially circular void collapses into one or more slits. Figure 7 illustrates this phenomenon. In the example shown, two slits emerge from an initially circular void, and propagate along the line. It has been suggested that this type of shape instability may be responsible for causing open circuits in the line. If a void collapses into a slit which is perpendicular to the line, then a void with a relatively small size may sever the interconnect. Our simulations suggest that slits collapse along a line rather than across it, in agreement with the results obtained by Bower and Freund (1995). Furthermore, shape instability may eventually cause a large void to break up into two or more smaller cavities, so reducing the changes of an open circuit.

The critical value of χ at which a void will collapse into a slit depends on the initial geometry of the cavity and on the geometry of the interconnect line. A circular void in an infinite, conducting solid is stable to first-order perturbations in its shape (Marder, 1994, as cited in Wang *et al.*, 1996). Therefore, if the void is perfectly circular, and is much smaller than the line width, it will remain circular. The void may collapse if its initial shape is appreciably non-circular: for example, Wang *et al.* (1996) have computed the critical value of χ at which an elliptical cavity will collapse, as a function of the eccentricity of the initial void. Here, we have calculated the value

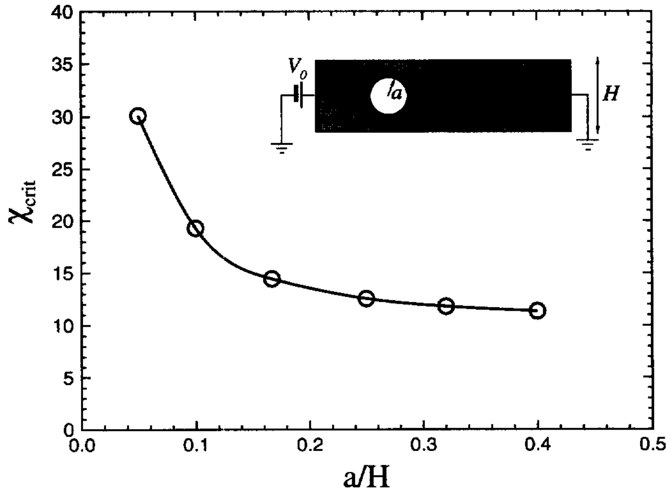

Fig. 8. The critical value of $\chi = V_0|e|Z^*a^2/\Omega\gamma_s L$ at which an initially circular cavity on the symmetry plane of an electrically conducting strip will collapse to slits.

of χ required to collapse an initially circular void which lies on the symmetry plane of an interconnect of height H, as a function of the ratio of the initial void size to the line width a/H. The result is displayed in Fig. 8.

4.3. *Void instability under stress*

The shape of a void in an interconnect is influenced not only by the electric current flow, but also by the distribution of stress in the line. Figure 9 shows a small circular

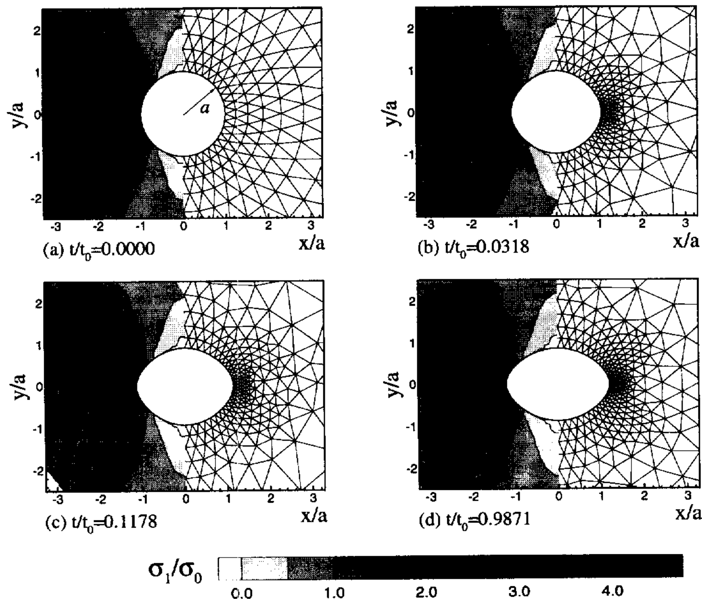

Fig. 9. Stable evolution of a circular cavity in an elastic solid under remote stress. Results are shown for $\Lambda = 0.2$, $\sigma_{xx} = 0$, $\sigma_y = \sigma_0$; contours show the distribution of maximum principal stress σ_1/σ_0.

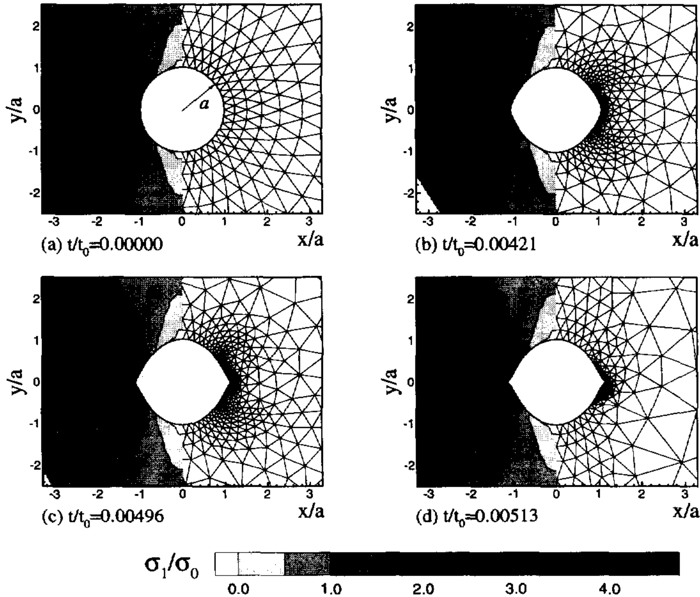

Fig. 10. Evolution of cracks from an initially circular void subjected to remote stress. Results are shown for $\Lambda = 0.6$, $\sigma_{xx} = 0$, $\sigma_{yy} = \sigma_0$; the characteristic time is $t_0 = a^4/\mathscr{D}_s\Omega\gamma_s$; contours show the distribution of maximum principal stress σ_1/σ_0.

cavity of radius a in an isotropic, linear elastic solid. The boundaries of the solid are subjected to normal tractions, which induce uniform principal stresses σ_{xx}, σ_{yy} remote from the void. The solid is free of electric current. Variations in strain energy around the void surface cause atoms to migrate from regions of high energy to those of low strain energy. This causes the void to change its shape, as shown in Fig. 9. Once the void changes its shape, the mass flux over its surface is opposed by variations in curvature. The relative magnitudes of the driving forces associated with deformation and surface energy may be quantified by a dimensionless parameter Λ:

$$\Lambda = \frac{(\sigma^{\infty})^2 a}{E\gamma_s}, \tag{4.7}$$

where σ^{∞} is the maximum principal stress remote from the void. For small values of Λ, surface energy dominates: in this case the void steels to an approximately elliptical shape, as shown in Fig. 9. If Λ exceeds a critical value, then the void collapses to a slit oriented perpendicular to the maximum principal stress (Suo and Wang, 1994). The initial stages of this process are shown in Fig. 10. The void first adopts an elliptical shape, then develops two noses, which subsequently sharpen.

There is evidence to suggest that these noses collapse to sharp cusps, with a singular curvature and strain energy density at the cusp tip (Suo and Wang, 1994; Wang and Suo, 1997). It is difficult to approach this limit using our numerical procedure, since singular states of stress are not represented accurately by our finite element interpolation scheme. However, we have performed careful numerical computations

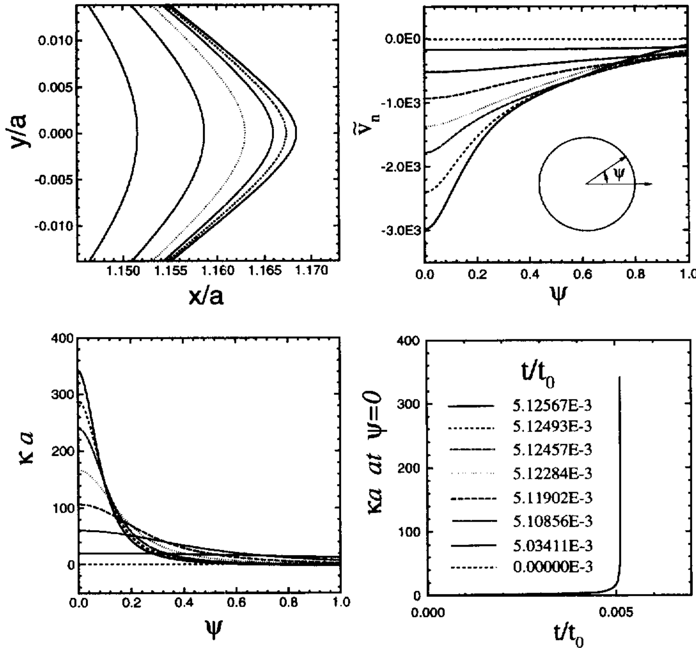

Fig. 11. Details of the emergence of a crack from an initially circular void. Results are shown for $\Lambda = 0.6$, $\sigma_{xx}/\sigma_{yy} = 0$. (a) Profiles of the tip of the notch, shown at successive intervals of time; (b) variation of the dimensionless normal velocity of the surface $\tilde{v}_n = v_n a^3/\mathcal{D}_s\Omega\gamma_s$; (c) the curvature of the surface of the void near the notch tip; (d) the variation of the maximum curvature at the notch tip with time.

to elucidate some of the features associated with the development of the cusps. Figure 11a shows successive profiles of the cavity in the region around one nose, as successive intervals of time. The variation in the normal velocity of the void surface near the tip of the nose is shown in Fig. 11b. Figure 11c shows the variation in curvature near the tip of the notch, while Fig. 11d shows the maximum curvature as a function of time. As the nose forms, both the velocity of the void tip and the maximum curvature increase extremely rapidly, suggesting that a crack will indeed emerge from the tip of the nose. This behavior is very similar to the roughening of a slightly non-planar surface due to strain energy driven surface diffusion. Detailed studies of crack formation in this system have been conducted by Chiu and Gao (1993, 1994) and by Gao (1995), among others. Of course, in practice, the formation of a sharp crack tip may be prevented by plastic deformation, either owing to dislocations emitted from the crack tip itself, or owing to dislocations nucleated from sources within the solid.

4.4. *Void instability under combined stress and electric field*

Finally, we investigate the behavior of a cavity in an interconnect under both stress and electric current flow. Consider a rectangular strip, height H and length L, which contains an initially circular void of radius a. An electric field is induced in the solid by prescribing the voltage at both ends of the strip: $V = V_0$ on $x = 0$, and $V = 0$ on

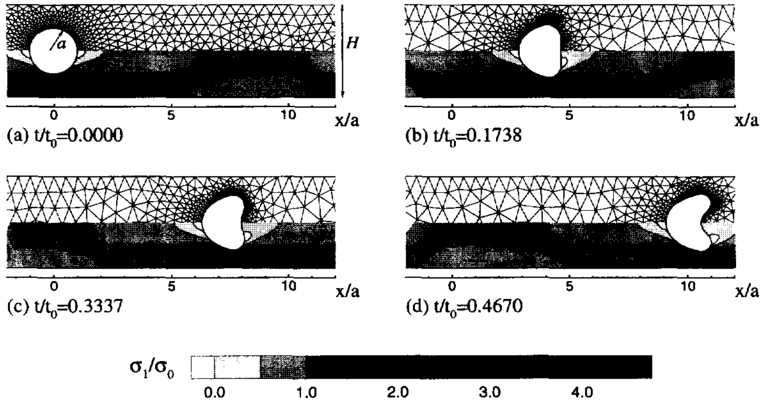

Fig. 12. Evolution of a void under combined stress and electric field. Results are shown for $\chi = 10$, $\Lambda = 0.1$, $\sigma_{xx} = \sigma_0$, $\sigma_{yy} = 0$. The characteristic time is $t_0 = a^4/\mathscr{D}_s\Omega\gamma_s$; contours show maximum principal stress σ_1/σ_0.

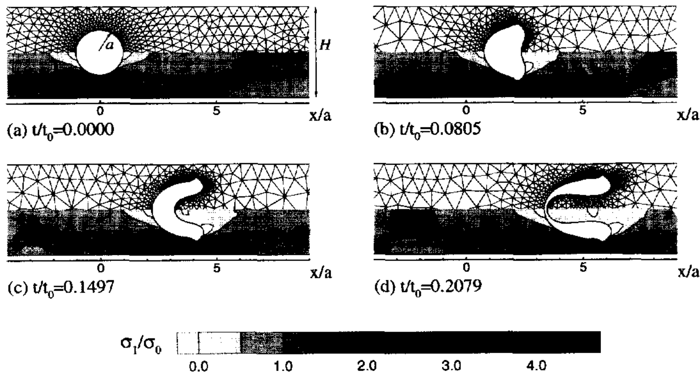

Fig. 13. A void collapsing into cracks under combined stress and electric field. Results are shown for $\chi = 10$, $\Lambda = 0.2$, $\sigma_{xx} = \sigma_0$, $\sigma_{yy} = 0$. The characteristic time $t_0 = a^4/\mathscr{D}_s\Omega\gamma_s$; contours show maximum principal stress σ_1/σ_0.

$x = L$. The faces $x = 0$, $x = L$ are subjected to normal tractions σ_{xx}, while the faces $y = 0$, $y = H$ are subjected to normal tractions σ_{yy}. The behavior of the void is now determined by the values of χ [equation (4.6)], Λ [equation (4.7)] and the ratio σ_{xx}/σ_{yy}, as well as the geometry of the solid a/H, L/H. For small values of both χ and Λ, surface energy dominates over all other driving forces for surface diffusion; the void then remains circular and migrates along the line, as discussed earlier. For large values of χ or Λ, both electromigration and strain energy variations in the solid tend to cause the void to develop slits or cracks. Electromigration and strain energy appear to act in a cooperative manner, so as to promote the emergence of cracks. For example, Fig. 12 shows the evolution of a void for $\chi = 10$ and $\Lambda = 0.1$, while Fig. 13 shows void evolution for $\chi = 10$ and $\Lambda = 0.2$. For $\Lambda = 0.1$, the void collapses into two lobes, as it would in the absence of stress. For $\Lambda = 0.2$, two cracks begin to emerge from the

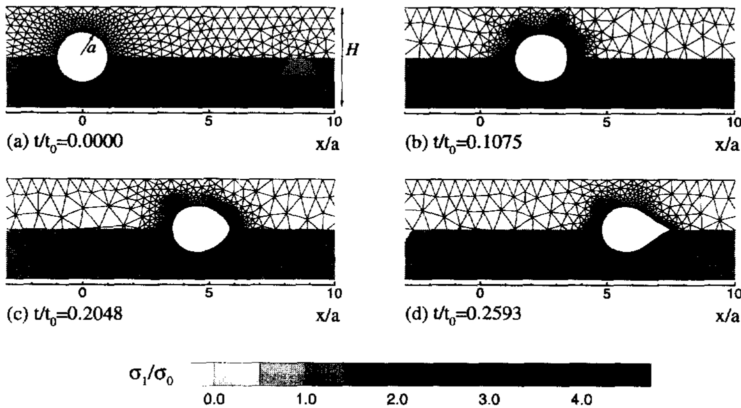

Fig. 14. A void collapsing into a crack under combined stress and electric field. Results are shown for $\chi = 10$, $\Lambda = 0.2$, $\sigma_{xx} = \sigma_{yy} = \sigma_0$. The characteristic time is $t_0 = a^4/\mathscr{D}_s\Omega\gamma_s$; contours show the distribution of maximum principal stress σ_1/σ_0.

tips of the lobes. Recall that in the absence of electric current, cracks form only when $\Lambda > 2/3$.

Stresses in interconnect lines are close to hydrostatic: it is interesting to observe the behavior of voids in the line under these conditions. Figure 14 shows results obtained with the normal tractions σ_{xx} and σ_{yy} equal, for $\chi = 10$ and $\Lambda = 0.2$. A single sharp nose emerges from the void in the direction of the line; the stress field is sufficient to suppress the two lobes that form in the absence of mechanical loading.

It is notable that we have not observed slits to form perpendicular to the lines in any of our simulations involving both electric current flow and stress. It is possible that elastic anisotropy, or anisotropy in the surface energy may promote the formation of such slits. The presence of grain boundaries in the line is also expected to influence the migration and evolution of the voids. These are promising areas for future work.

ACKNOWLEDGEMENTS

This work was supported by the Materials Research Group on Micromechanics of Failure Resistant Materials at Brown University, which is funded by the National Science Foundation under grant No. DMR-9223683. A.F.B. is also grateful for support from O.N.R. through contract N00014-95-1-0239; L.X. and C.F.S. are pleased to acknowledge support from O.N.R. contract N00014-95-1-0399. Z.S. is grateful for support from the National Science Foundation through grant MSS 9202165.

REFERENCES

Arzt, E., Kraft, O., Nix, W. D. and Sanchez, J. E. (1994) Electromigration failure by shape change of voids in bamboo lines. *J. Appl. Phys.* **76**, 1563.

Bower, A. F. and Freund, L. B. (1993) Analysis of stress induced void growth mechanisms in passivated interconnect lines. *J. Appl. Phys.* **74**, 3855–3868.

Bower, A. F. and Freund, L. B. (1995) Finite element analysis of electromigration and stress

induced diffusion in deformable solids. *Materials Reliability in Microelectronics V*, ed. A.S. Oates, W.F. Filter, R. Rosenberg, A. Lindsay Greer and K. Gadepally. Materials Research Society Proc. Vol. **391,** pp. 177–188.

Cavendish, J. C. (1974) Automatic triangulation of arbitrary planar domains for the finite element method. *Int. J. Num. Methods in Engng* **8,** 679–696.

Chiu, C.-H. and Gao, H. (1993) Stress singularities along a cycloid rough surface. *Int. J. Solids Struct.* **30,** 2983–3012.

Chiu, C.-H., and Gao, H. (1994) Numerical simulation of diffusion controlled surface evolution. *Mater. Res. Soc. Symp. Proc.* **317,** 369–374.

Cocks, A. C. F. (1989) A finite element description of grain boundary diffusion processes in ceramic materials. *Applied Solid Mechanics* 3, ed. I.M. Allison and C. Ruiz. North Holland, Amsterdam.

Cocks, A. C. F. and Gill, S. P. A. (1996) A variational approach to two dimensional grain growth. *Acta Metall. Mater.* to appear.

Cocks, A. C. F. and Searle, A. A. (1991) Void growth by grain boundary diffusion in fine grained materials. *Mech. Mater.* **12,** 279–287.

Gao, H. (1995) Mass conserved morphological evolution of hypocycloid cavities: a model of diffusive crack initiation with no associated energy barrier. *Proc. R. Soc. Lond.* **A448,** 732–734.

Hasunuma, M., Toyoda, H., Kawanoue, T., Ito, S., Kaneko, H. and Miyauchi, M. (1995) A highly reliable Al line with controlled texture and grain boundaries. In *Materials Reliability in Microelectronics V*, ed. A.S. Oates, W.F. Filter, R. Rosenberg, A. Lindsay Greer and K. Gadepally. Materials Research Society Proc. Vol. **391,** pp. 335–346.

Hinton, E. and Campbell, J. (1974) Local and global smoothing of discontinuous finite element function using a least squares method. *Int. J. Num. Methods in Engng.* **8,** 461–480.

Ho, P. S. (1970) Motion of inclusion induced by a direct current and a temperature gradient. *J. Appl. Phys.* **41,** 64–68.

Korhonen, M. A., Paszkiet, C. A. and Li, Che-Yu (1991a) Mechanisms of thermal stress relaxation and stress induced voiding in narrow aluminium based metallizations. *J. Appl. Phys.* **69**(12), 8083.

Korhonen, M. A., LaFontaine, W. R., Borgesen, P. and Li, Che-Yu, (1991b) Stress induced nucleation of voids in narrow aluminium-based metallizations on silicon substrates. *J. Appl. Phys.* **70,** 6774.

Lohner, R. (1988) Some useful data structures for the generation of unstructured grids. *Commun. Appl. Num. Methods* **4,** 123–135.

Marieb, T., Bravman, J. C., Flinn, P. and Madden, M. (1994) *In situ* observations of voiding in metal lines under passivation. *Mater. Res. Soc. Symp. Proc.* **338,** 409–413.

Needleman, A. and Rice, J. R. (1980) Plastic creep flow effects in the diffusive cavitation of grain boundaries. *Acta Metall.* **28,** 1315–1332.

Oden, J. T. and Reddy, J. N. (1973) Note on approximation method for computing consistent conjugate stresses in finite elements. *Int. J. Num. Methods in Engng.* **6,** 55–61.

Pan, J. and Cocks, A. C. F. (1995) A numerical technique for the analysis of coupled surface and grain boundary diffusion. *Acta Metall. Mater.* **43,** 1395–1406.

Peraire, J., Vahdati, M., Morgan, K. and Zienkiewicz, O. C. (1987) Adaptive remeshing for compressible flow computations. *J. Comp. Phys.* **72,** 449–466.

Riege, S. P., Hunt, A. W. and Prybyla, J. A. (1995) Real time TEM studies of electromigration in submicron aluminum runners. In *Materials Reliability in Microelectronics V*, ed. A.S. Oates, W.F. Filter, R. Rosenberg, A. Linday Greer and K. Gadepally. Materials Research Society Proc. Vol. **391,** pp. 249–258.

Suo, Z. and Wang, W. (1994) Diffusive void bifurcation in stressed solid. *J. Appl. Phys.* **76,** 3410–3421.

Wang, W. Q. and Suo, Z. (1997) Shape change of a pore in a stressed solid via surface diffusion motivated by surface and elastic energy variation. *J. Mech. Phys. Solids* **45**(5), 709.

Wang, W. Q., Suo, A. and Hao, T. H. (1996) A simulation of electromigration induced transgranular slits. *J. Appl. Phys.* **79**(5), 2394–2403.

Yang, W., Wang, W. and Suo, Z. (1994) Cavity and dislocation in instability under electric current. *J. Mech. Phys. Solids* **42,** 897–911.

APPENDIX

For convenience, we list below the finite element interpolation functions used to solve (3.8). Let $j_s(s)$ denote the variation of flux with arc length over the surface of the void. Suppose that the $s^{(i)}$, with $i = 1, 2, \ldots, N$ denote the position of N discrete points on the void surface, with $s^{(i-1)} < s^{(i)} < s^{(i+1)}$. Let $j_s^{(i)}$ denote the value of the flux at the ith point, and let $v_n^{(i)}$ denote the velocity of the void surface ($v_n = -\mathrm{d}j_s/\mathrm{d}s$) at $s = s^{(i)}$. Over the region $s^{(i)} < s < s^{(i+1)}$, we then interpolate j_s as

$$j_s(s) = N_1(s)j_s^{(i)} + N_2(s)v_n^{(i)} + N_3(s)j_s^{(i+1)} + N_4(s)v_n^{(i+1)},$$

where

$$N_1(s) = (1-\xi)^3(1+3\xi+6\xi^2) \quad N_2(s) = -h\xi(1-\xi)^3(1+3\xi)$$

$$N_3(s) = \xi^3(10-15\xi+6\xi^2) \quad N_4(s) = -h\xi^3(1-\xi)(3\xi-4)$$

with $h = s^{(i+1)} - s^{(i)}$ and $\xi = (s-s^{(i)})/h$.